Evidence for a dimensionality crossover at the disappearance of magnetism in the Kondo lattice alloy $CeCo_{1-x}Fe_xSi$

J. G. Sereni, M. Gomez Berisso, D. Betancourth, and V. F. Correa
Low Temperature Division, CAB-CNEA and CONICET, 8400 San Carlos de Bariloche, Argentina

N. Caroca Canales and C. Geibel
Max-Planck Institute for Chemical Physics of Solids, D-01187 Dresden, Germany

(Received 15 September 2013; revised manuscript received 18 November 2013; published 7 January 2014)

Structural, magnetic, and thermal measurements performed on $CeCo_{1-x}Fe_xSi$ alloys are reported. Three regions can be recognized: (i) Co rich ($x \leqslant 0.20$) with a decreasing long-range antiferromagnetic order which vanishes at finite temperatures, (ii) an intermediate region ($0.20 < x \leqslant 0.30$) showing a broad magnetic anomaly (C_A) in specific heat, and (iii) the nonmagnetic region progressively changing from a non-Fermi-liquid-type behavior towards a Fermi-liquid one as Fe concentration increases. The C_A anomaly emerges as an incipient contribution above T_N already at $x = 0.10$, which indicates that this contribution is related to short-range correlations likely of quasi-two-dimensional type. Both T_N transition and C_A anomaly are practically unaffected by an applied magnetic field up to $B \approx 10$ T.

DOI: 10.1103/PhysRevB.89.035107 PACS number(s): 71.27.+a, 71.10.Hf, 75.30.Mb, 75.30.Kz

I. INTRODUCTION

Magnetic correlations play an important role in systems undergoing phase transformations.[1] Besides canonical thermal fluctuations driving a three-dimensional (3D) magnetic system into a long-range magnetic order (LR-MO) ground state (GS), there are different types of fluctuations allowing for the exploration of alternative minima for its free energy. For example, novel exotic phases may occur as alternative GSs due to geometrical frustration.[2] Low dimensionality is another factor that enhances fluctuations due to geometrical constraints on the propagation of the order parameter.

In rare-earth-based intermetallic compounds, magnetic interactions are driven mainly by the well-known Ruderman-Kittel-Kasuya-Yosida (RKKY) mechanism, which is essentially of 3D character. Although real low dimensionality is unlikely in intermetallic compounds, strongly anisotropic structures, such as in those resembling multilayer structures,[3] favor similar effects. Among Ce-equiatomic ternaries, CeFeSi- and CeScSi-type structures provide the possibility to explore that alternative. The tetragonal CeFeSi-type structure builds up from two consecutive planes of Ce ions located in a simple squared lattice (with Tungsten-type atomic configuration) stacked up along the "c" direction with $BaAl_4$-type blocks, following the Ce-Ce-Si-Fe_2-Si-Ce-Ce sequence shown in Fig. 1.

In this paper, we report on structural, magnetic, and thermal properties of $CeCo_{1-x}Fe_xSi$ alloys investigated all along the concentration range. The respective stoichiometric limits are the antiferromagnetic CeCoSi [$T_N = 8.8$ K (Ref. 4)] with localized $4f$ moments and the nonmagnetic CeFeSi showing intermediate valent behavior.[5] Thus, this system allows running through a critical region where magnetic order vanishes.

II. EXPERIMENTAL RESULTS

A. Sample preparation and techniques

Polycrystalline samples of $CeCo_{1-x}Fe_xSi$ with $0 \leqslant x \leqslant 1$ were synthesized by arc melting the nominal amounts of the constituents (purity above 99.99%) under an argon atmosphere weighted inside an Ar atmosphere glovebox. The samples were turned and were remelted several times to ensure homogeneity. Then, the samples were placed in a tungsten boat wrapped with zirconium foil and annealed at 1200 °C for 1 week. The quality of the samples was verified by means of x-ray powder-diffraction measurements using Cu $K\alpha_1$ radiation ($\lambda = 1.540\,56$ Å) in a Stoe-Stadip-MP diffractometer. The pattern was indexed on the basis of the tetragonal CeFeSi-type structure. Eleven samples were studied all along the concentration range.

Specific heat was measured using a standard heat-pulse technique in a semiadiabatic He^3 calorimeter in the range between 0.5 and 25 K at zero and applied magnetic fields of $\mu_0 H = 4$ T in some selected samples. The magnetic contribution C_m is obtained by subtracting the phonon contribution extracted from LaCoSi. Dc-magnetization measurements were carried out using a Quantum Design magnetic property measurement system (superconducting quantum interference device) magnetometer operating between 2 and 300 K and as a function of the field up to 5 T. Electrical resistivity was measured between 2 K and room temperature using a standard four-probe technique with an LR700 bridge. A high-resolution ($\leqslant$ 1-Å) capacitive dilatometer[6] was used in the thermal-expansion experiments.

B. Structural properties

The relevant interatomic distances in the CeFeSi-type structure are the following: d_{T-X}, d_{R-T}, and d_{R-X}, R being the rare earth (Ce in this case), T being the transition metal (Co/Fe), and X being the semimetal (Si), see Fig. 1. The crystal chemistry study performed on the isotypic compound LaFeSi (Ref. 7) indicates a reduction in the mentioned distances with respect to the corresponding values of the pure elements. The respective relative dilatations $\Delta_{i-j} = [d_{i-j} - (r_i + r_j)]/[(r_i + r_j)] \times 100$ with r_i as the elemental radii are as follows: $\Delta_{\text{Fe-Si}} = -8.1\%$, $\Delta_{\text{La-Fe}} = -2.7\%$, and $\Delta_{\text{La-Si}} = -3.4\%$, whereas, the other distances: $d_{\text{Fe-Fe}}$, $d_{\text{Si-Si}}$,

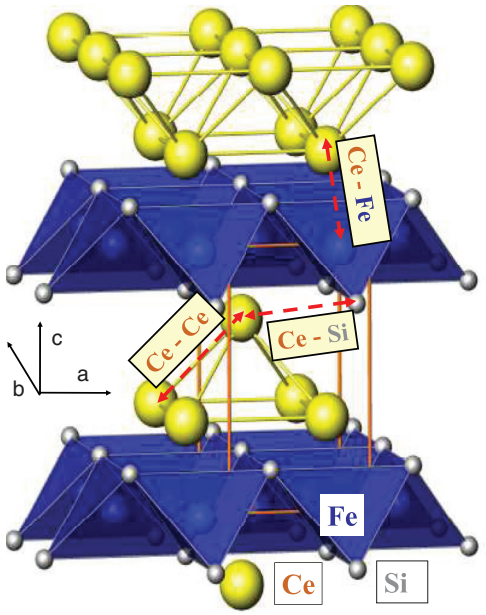

FIG. 1. (Color online) Tetragonal CeFeSi-type structure with the relevant interatomic distances among Ce-Ce, Ce-Si, and Ce-Fe atoms. Individual atoms are identified on the lower plane.

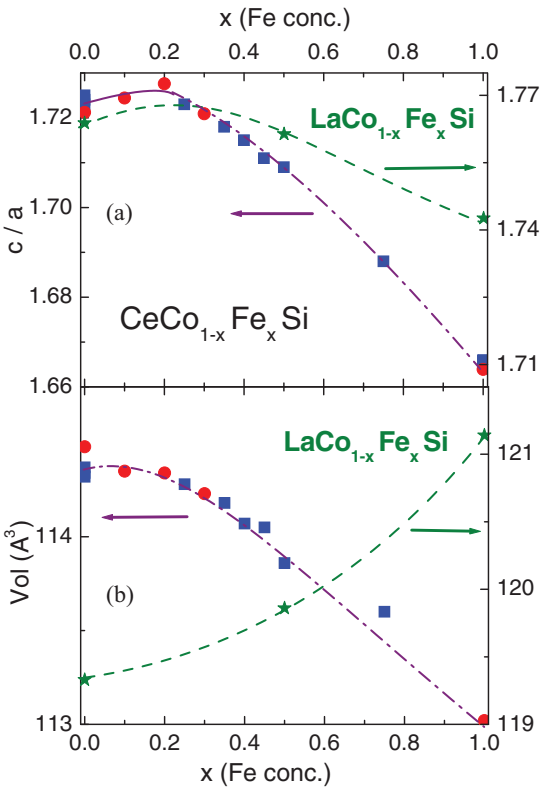

FIG. 2. (Color online) (a) c/a lattice parameters ratio and (b) unit-cell volume variation as a function of Fe content in $CeCo_{1-x}Fe_xSi$ (left axis). Blue squares and red dots identify two different sets of samples. Respective reference parameters from $LaCo_{1-x}Fe_xSi$ are included (green) using the right axis. Dashed-dotted and dashed curves are guides for the eye.

and $d_{\text{Ce-Ce}}$ increase. The large contraction observed on $d_{\text{Fe-Si}}$ is related to a strong electronic hybridization between those atoms. This explains the nonmagnetic behavior of Fe (or Co) atoms as a consequence of a large bandwidth.

In the system under study, two regions can clearly be distinguished in the concentration dependence of the lattice parameters, see Fig. 2. On the Co-rich side, there are minor variations up to about 20% of Fe doping. Beyond that concentration, a clear modification occurs in the variation of both tetragonal axes: $a(x)$ increases about 1%, whereas, $c(x)$ decreases about 5% once it reaches the CeFeSi stoichiometric limit. Figure 2(a) shows a significant reduction in the c/a ratio (about 3.5%), coincident with a decrease in the unit-cell volume (about 1.3%), shown in Fig. 2(b). This structural variation tends to reduce Ce-Ce spacing $d_{\text{Ce-Ce}}$ between neighbors placed on the apex and on the square-base pyramids formed by adjacent Ce layers.

The volume variation above $x \approx 0.20$ [see Fig. 2(b)] largely exceeds the equivalent variation for neighboring lanthanides (i.e., La and Pr) as a sign of the Ce-4f orbitals' instability with Fe content. As a reference, the respective values of three La(Co,Fe)Si samples are included in Figs. 2(a) and 2(b) on the right axis. The increase in volume between LaTSi (T = Co and Fe) compounds contrasts with the strong decrease in $CeCo_{1-x}Fe_xSi$ alloys, indicating the collapse of the Ce atomic volume for $x \geqslant 0.20$. In fact, the CeCoSi unit-cell volume is $\approx$1% below the interpolation between LaCoSi and PrCoSi, whereas, CeFeSi is $\approx$4% below the equivalent La to Pr interpolation.[8]

C. Magnetic properties

The inverse of the high-temperature magnetic susceptibility is presented in Fig. 3(a) as $\mu_0 H/M$. Above $T \geqslant 50$ K, it shows a Curie-Weiss-type thermal dependence of $\chi = C_c/(T + \theta_P)$, where the Curie constant is $C_c = N\mu_{\text{eff}}^2/3k_BT$ with μ_{eff} as the effective magnetic moment. The extracted μ_{eff} values range between $2.67\mu_B$ for $x = 0.10$ and $2.45\mu_B$ for $x = 0.32$, which are close to the $J = 5/2$ Hund's rule ground-state value of $2.54\mu_B$ predicted for Ce^{3+} atoms. For an increasing Fe concentration, μ_{eff} decreases in coincidence with the increase in the paramagnetic temperature $\theta_P(x)$ as presented in the inset of Fig. 3(a). Higher Fe concentration samples show low-temperature ferromagnetic contributions that become important as the main magnetization decreases. This likely is related to a small amount of the ferromagnetic Fe-impurity phase.

The relatively high value of θ_P at low Fe content is likely due to a combination of the Kondo effect acting on respective excited crystal-electric-field (CEF) levels and RKKY interactions. However, the upturn in $-\theta_P(x)$ beyond $x = 0.25$ is dominated by the increase in Kondo interaction related to the significant volume reduction. A corresponding Kondo temperature (T_K) can be evaluated following the Krishna-Murthy criterion: $T_K = -\theta_P/2$.[9]

Details for the low-temperature magnetic behavior are presented in Fig. 3(b), showing the shift in the maximum of $M(T)$ and the related antiferromagnetic ordering from $T_N = 9$ K at $x = 0$ down to $\approx$2 K at $x = 0.30$. The latter hardly is seen in Fig. 3(b) because it contains curves obtained with an applied magnetic field of $\mu_0 H = 1$ T, albeit the

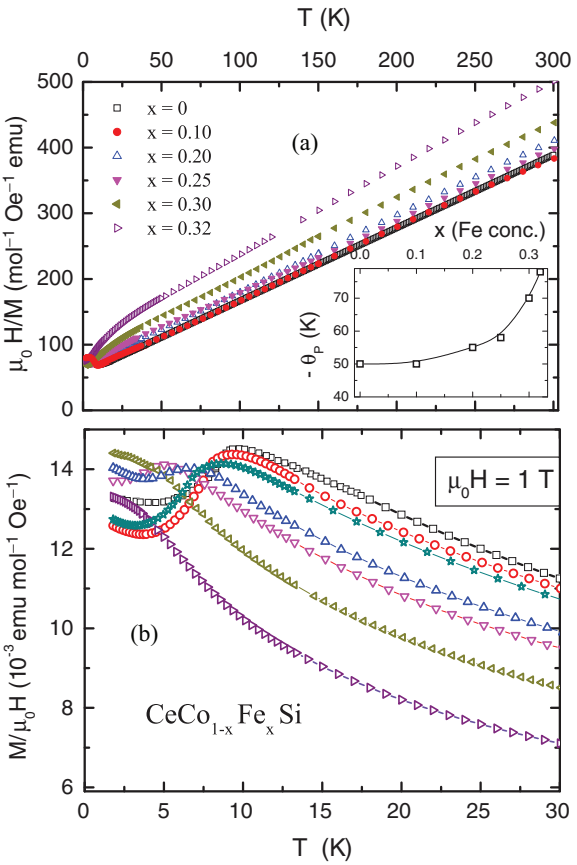

FIG. 3. (Color online) (a) High-temperature inverse of magnetic susceptibility for $0 \leqslant x \leqslant 0.32$. Data of CeCoSi were extracted from Ref. 4. Inset: paramagnetic temperature θ_P as a function of Fe concentration extrapolated from $T < 50$ K. (b) Low-temperature susceptibility showing the shift in the maximum connected with the antiferromagnetic order at low temperatures with increasing Fe content.

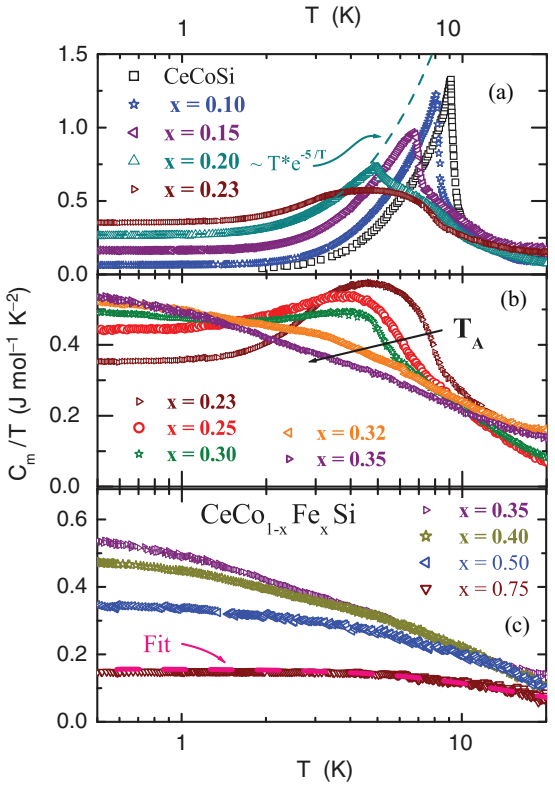

FIG. 4. (Color online) Specific heat divided by temperature of all studied samples in a logarithmic representation. (a) The Co-rich side ($0 \leqslant x \leqslant 0.20$) showing the decreasing specific heat jump at the magnetic transition. Dashed curve: fit with a $C_m/T(x = 0.20) \propto T$ dependence. (b) The $0.23 \leqslant x \leqslant 032$ range where the C_A anomaly becomes dominant (see the text). The arrow indicates the temperature T_A at the maximum $\partial C_A/\partial T$ slope. (c) The nonmagnetic region for $x \geqslant 0.35$ including the fit (dashed curve) with a Kondo-type temperature dependence.[11]

maximum clearly is observed in a lower applied field, e.g., $\mu_0 H = 0.03$ T (not shown). For lower Fe concentrations, the strength of the applied magnetic field does not produce relevant variations around the magnetic transition. Beyond $x = 0.30$, no cusp can be discerned even at the lowest field. Instead of that, a continuous increase in $M(T)$ with decreasing T that converges towards a constant value at the lowest measured temperature is observed.

D. Specific heat

The magnetic contribution to the specific heat (C_m) is obtained after subtracting the phonon contribution extracted from the isotypic La compound. The results of all studied samples are collected in Fig. 4. Three distinct behaviors are observed in different concentration ranges: (a) on the Co-rich side with a rapid decrease in the $C_m(T_N)$ jump $\Delta C_m(T_N)$ within the $0 \leqslant x \leqslant 0.20$ concentration range, (b) a broad anomaly (C_A) that becomes dominant between $x = 0.23$ and 0.32, and (c) a nonmagnetic region for $x \geqslant 0.35$. Although these three regions are clearly distinguishable, the onset of the $C_A(T)$ anomaly already is detected at lower Fe concentrations right above the $T_N(x)$ transition. Notably, this incipient anomaly starts to develop at $T \approx 10 \approx T_N(x = 0)$ K. This fact indicates that the anomaly builds up from the same type of antiferromagnetic (AFM) correlations but changing from long range to short range (SR) as the magnetic coupling in the c direction weakens.

As the $\Delta C_m(T_N)/T$ jump weakens and the C_A anomaly becomes dominant, an underlying Kondo-type contribution also arises. This contribution is related to the formation of heavy fermion (HF) quasiparticles. The low-temperature value of this HF contribution increases continuously with x as indicated by the $C_m/T|_{\lim T\to 0}(x)$ values. At $x = 0.35$, a non-Fermi-liquid- (NFL-) type dependence: $C_m/T \propto -\ln(T)$ clearly is observed, although it tends to flatten at low temperatures. This temperature dependence is predicted by theory[10] to occur close to a quantum phase transition in a two-dimensional (2D) itinerant AFM system.

For $x > 0.5$, a progressive transformation into a Fermi-liquid regime occurs as the Ce lattice enters into an intermediate valence regime concomitant with the Ce-volume reduction. In Fig. 4(c), we show the fit for sample $x = 0.75$ performed using a Kondo-impurity-type temperature dependence with $T_K = 56$ K. This value is consistent with $C_m/T(T \to 0) = 0.15\ \mathrm{J\,mol^{-1}\,K^{-2}}$ accounting for the fact that $C_{\mathrm{imp}}/T(T \to$

$0) = (R\pi/3) \times (8.7/T_K)$ (Ref. 11) and the temperature at which 2/3 of the R ln 2 entropy is reached.

The temperature of the specific heat jump at T_N does not coincide with the maximum of $M(T)$ but with the maximum of its $\partial M/\partial T$ derivative. This difference typically occurs in low-dimensional or strong anisotropic magnetic systems,[1] however, this is not enough to prove low dimensionality.[12]

III. DISCUSSION

A. Interatomic spacing

In order to understand the complex behavior of this system, we start by discussing the modification of the volume of the unit cell driven by the Co/Fe substitution. The simple comparison between volumes of CeCoSi and CeFeSi with the interpolation between the respective La and Pr isotypic neighbors shows a volume collapse of about 3%.[8] This reduction in the unit-cell volume between Ce(Co/Fe)Si stoichiometric limits is the fingerprint of valence instability where the Ce-4f electron delocalizes allowing the atomic volume collapse through an eventual $4f$-$3d$ hybridization. Notably, $d_{\text{Ce-Si}}$ slightly increases following the increase in the a parameter. The same analysis can be performed on the c/a ratio, see Fig. 2(b), indicating that the collapse is reflected mostly in the c axis. Since the size of the ligand atoms in the T-Si layers does not change significantly, the strong reduction in the c axis can be attributed to the Ce atoms' volume reduction. Concerning Ce-Ce spacing, the reduction in the c axis with Fe concentration reflects the decrease in the Ce-Ce distance between two consecutive layers, which, in CeFeSi, is 3.693 Å, in comparison with the on-plane Ce-Ce neighbors at 4.026 Å.[8] The later distance is related to the increase in the a axis.

B. Phase diagram

The concentration dependence of the relevant parameters is summarized in a schematic phase diagram in Fig. 5. It includes the $T_N(x)$ decrease together with the respective specific heat jump $\Delta C_m(T_N)/T$ reduction that vanishes at $x = 0.23$. The decreasing height of $\Delta C_m/T$ at $T = T_N(x)$ is qualitatively represented in the figure as a segment attached to each point. The $C_A(T)$ anomaly is represented by the characteristic temperature $T_A(x)$ defined in Fig. 4(b) as the temperature of the maximum negative $\partial C_A/\partial T$ slope above $T_N(x)$. The HF component is represented by the C_m/T values at $T = 0.5$ K, which increases in the region of $0 < x < 0.35$ where degrees of freedom are transferred progressively from the ordered phase into the heavy quasiparticles. Beyond that concentration, C_m/T decreases with x since, $C_m/T \propto 1/T_K$, the Kondo temperature increases as expected for a nonordered Kondo lattice.

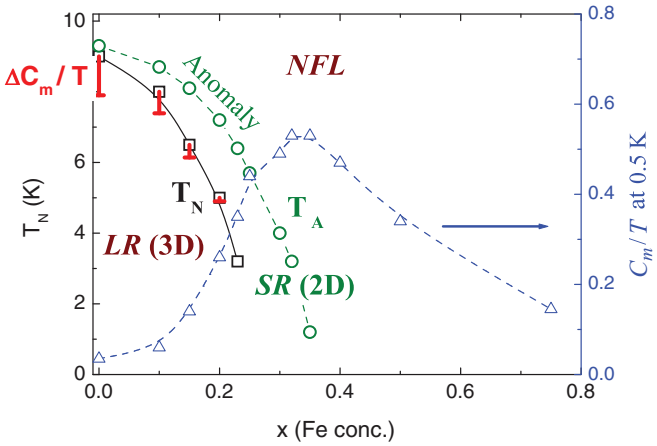

FIG. 5. (Color online) Phase diagram collecting (□) $T_N(x)$ with (red) bars representing the jump $\Delta C_m(T_N)$. The lower $T_N(x = 0.23)$ point indicates the temperature of the deviation from the AFM behavior as $\Delta C_m(T_N) \to 0$. (◯) $T_A(x)$ represents the characteristic temperature of the onset of the broad anomaly, defined in Fig. 4(b). (△) $C_m/T(x)$ values at 0.5 K.

C. On the nature of the specific heat anomaly

The origin and nature of the $C_A(T)$ anomaly deserve a more detailed analysis. As mentioned before, it emerges like a $T > T_N(x)$ tail as soon as $T_N(x)$ starts to decrease and is fully developed once the LR-MO phase is suppressed before the Kondo effects start to dominate the low-temperature behavior. One notices that the temperature dependence $C_m \propto T^2$, observed below $T_N(x)$, remains unchanged despite the decrease in $\Delta C_m/T_N$. As a reference, in Fig. 4(a), the fit with a $C_m/T = 0.27 + 0.3 \times T \times \exp(-5/T)$ dependence for $x = 0.20$ is included. The exponential factor reveals a gap in the magnon spectrum originating in the strong magnetic anisotropy. These features indicate that the $C_A(T)$ anomaly builds up from the same type of magnetic correlations, which at lower Fe concentration, are involved in the LR-MO phase formation. This anomaly very likely corresponds to short-range magnetic correlations of quasi-2D type within the double Ce layer. The increasing Kondo interaction and the atomic disorder in the Co/Fe-Si layer in between very likely results in a weakening of the magnetic interactions along the c direction and then to a crossover from a 3D to a quasi-2D system. This is in line with the NFL dependence $C_m/T \propto -\ln(T)$ observed for higher Fe concentration alloys.

In order to gain insight into the characteristics of this anomaly, we have performed thermal expansion (α) measurements at a zero field and under a high magnetic field ($\mu_0 H = 10, 16$ T) on sample $x = 0.15$. At that Fe concentration, both the incipient C_A anomaly and the T_N transition are competing, see Fig. 6(a). For comparison, zero-field electrical resistance (R) and specific heat at zero and $\mu_0 H = 4$ T magnetic field are included in Fig. 6(b). The temperature dependence of these three properties coincide in showing the onset of the anomaly contribution at $T \approx 12.5$ K, $\alpha(T)$ being the more sensitive one to the appearance of those magnetic correlations. Incipient coherence effects are observed in the $R(T)$ dependence starting at $T \approx 13$ K in coincidence with the onset of the $C_m(T)$ upturn above the magnetic transition. Further studies concerning magnetostriction and magnetoresistivity are in progress.

Notably, the applied magnetic field of $\mu_0 H = 4$ T produces no effects on $C_m(T)$, neither on the T_N transition nor on the anomaly, see Fig. 6(b). The same occurs with $\alpha(T)$ for $\mu_0 H = 4$ T (not shown), however, at $\mu_0 H = 10$ T, the anomaly in $\alpha(T)$ at $T \approx 13$ K strongly weakens but without affecting the T_N transition [see Fig. 6(a)], such as in stoichiometric

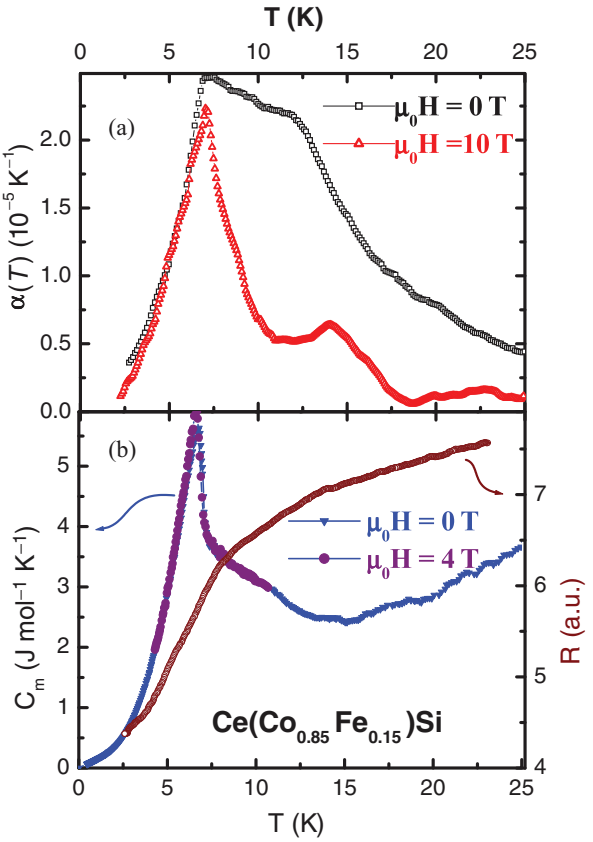

FIG. 6. (Color online) (a) Thermal expansion at zero and high magnetic fields in the longitudinal configuration ($L \parallel H$) of sample $x = 0.15$. (b) Comparison with zero-field electrical resistance (right axis) and specific heat with $\mu_0 H = 0$ and 4 T.

CeCoSi.[13] Only a slight shift in the transition to lower temperature (to $T_N \approx 5$ K) is observed at an applied field of 16 T. Concerning $M(B)$ measurements on this sample, a weak upturn occurs from a linear dependence for $B \geqslant 4$ T with almost identical results for $T = 1.8$, 3, and 5 K (see also, below).

The full $C_A(T)$ anomaly was investigated applying a magnetic field ($\mu_0 H = 4$ T) on sample $x = 0.23$ without detecting any field effect there. Interestingly, the field-dependent magnetization shows a slight upturn for $\mu_0 H > 3$ T, see Fig. 7, with a maximum deviation at $T \approx 6$ K as an indication of an incipient metamagnetic transition.

D. Entropy

In Fig. 8, we show the thermal variation in the entropy $S_m(T)$ along the full range of concentration. Also, in this parameter, two regions can be distinguished: (i) $0 < x < 0.25$ and (ii) $0.30 \leqslant x$. In the former, the entropy above 9 K is almost independent of concentration. Furthermore, $S_m(T)$ exceeds R ln 2 at around 12 K as a clear indication that the first excited CEF level is below 100 K and might contribute, to a small extent, to the low-temperature magnetism. From the $S_m(T)$ dependence, one can estimate the energy scale (T_0) of the interactions, which determine the low-temperature behavior of the $4f$ moments. Here T_0 is extracted from the temperature

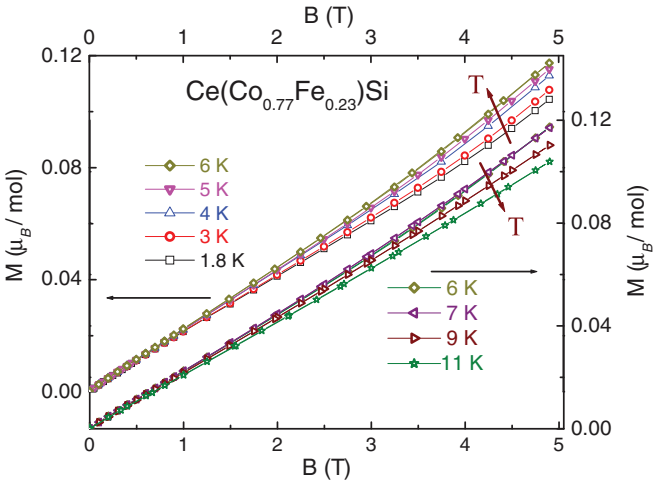

FIG. 7. (Color online) Magnetization isotherms of sample $x = 0.23$ up to $\mu_0 H = 5$ T showing an incipient metamagnetic transition above 3 T in the temperature region of the anomaly. For clarity, 6–11-K isotherms are shifted and are referred to the right axis.

at which $S_m(T)$ reaches $2/3(R \ln 2)$ because, for the single-ion Kondo model, it corresponds to T_K.[11] The alternative proposed by other models to evaluate T_K at the temperature at which $S_m(T)$ reaches $1/2(R \ln 2)$ is not applicable in this case because, for low Fe concentration, the S_m value corresponds to $T < T_N$ where RKKY interactions are present.

However, a general description of all interactions acting on the $4f$ moments at low temperatures should involve the sum of all of them, such as those that originated in the RKKY interactions and Kondo effect. In the inset of Fig. 8, the concentration dependence $T_0(x)$ is included showing that, for the present system, the dominant interactions at low Fe content (i.e., $x \leqslant 0.25$) are RKKY and, thus, $T_0 \approx T_{\mathrm{RKKY}}$. Increasing x above 0.30, the Kondo interaction becomes dominant, and then $T_0 \approx T_K$. This implies that, for small Fe content, T_K is

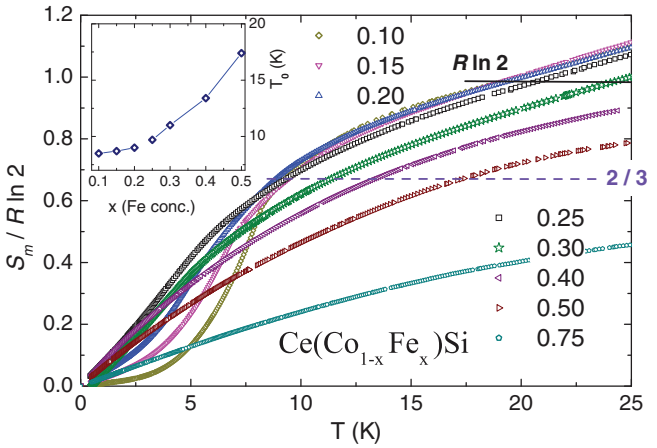

FIG. 8. (Color online) Thermal variation in the entropy normalized to the value of a doublet ground state. Inset: energy scale (T_0) of the exchange interactions acting on the $4f$ moments as deduced from $S_m(T)$ (see the text). For $x < 0.25$, it is dominated mainly by the RKKY interaction, whereas, for $x \geqslant 0.30$, it is dominated mainly by the Kondo effect.

below 7 K but increases strongly for $x > 0.30$ in accordance with the other physical properties.

IV. SUMMARY

Although the magnetic order of this system weakens with the Fe content, the phase boundary of the long-range magnetic order vanishes at finite temperatures with a progressive substitution of the LR-MO by short-range correlations. A broad anomaly (C_A) arises between the $T_N(x = 0)$ temperature and the actual decreasing $T_N(x)$ of each alloy. These features suggest that the involved AFM correlations change from LR-AFM to SR-AFM, likely of 2D character. Notably, the magnetic interactions in this system are very robust against external magnetic-field application because both the C_A anomaly and the $\Delta C(T_N)$ jump require $B \geqslant 10$ and $B \geqslant 14$ T to be suppressed or to be shifted, respectively.

Beyond the concentration region where the C_A anomaly occurs, the specific heat shows how the localized magnetic degrees of freedom on the Co-rich side are transferred to a heavy quasiparticle component exhibiting a NFL-type behavior. Once the NFL regime is reached around $x \approx 0.35$, T_K increases rapidly towards the Fe-rich side. The temperature dependence of the entropy, which exceeds R ln 2 already at 20 K for $x < 0.30$, indicates that the first excited CEF level lies below 100 K, and likely, it will get involved in the formation of the paramagnetic ground state. This results in a fast increase in the ground-state effective degeneracy. Further studies applying strong magnetic fields are in progress to better elucidate the exotic characteristics of the C_A anomaly and the significant magnetic hardness of these alloys.

This investigation confirms that Ce-equiatomic ternary compounds with strongly anisotropic structures allow accessing novel behaviors where enhanced fluctuations can play an important role.

ACKNOWLEDGMENTS

This work was partially supported by PICTP-2007-0812 and the Universidad de Cuyo 06/C393 projects.

[1]See, for example, J. L. De Jongh and A. R. Miedema, Adv. Phys. **23**, 1 (1974).
[2]J. Vannimenus and G. Toulouse, J. Phys. C **10**, L537 (1977).
[3]R. Welter, G. Venturini, E. Ressouche, and B. Malaman, J. Alloys Compd. **210**, 279 (1994).
[4]B. Chevalier and S. F. Matar, Phys. Rev. B **70**, 174408 (2004).
[5]R. Welter, G. Venturini, and B. Malaman, J. Alloys Compd. **189**, 49 (1992).
[6]G. M. Schmiedeshoff, A. W. Lounsbury, D. J. Luna, S. J. Tracy, A. J. Schramm, S. W. Tozer, V. F. Correa, S. T. Hannahs, T. P. Murphy, E. C. Palm, A. H. Lacerda, S. L. Bud'ko, P. C. Canfield, J. L. Smith, J. C. Lashley, and J. C. Cooley, Rev. Sci. Instrum. **77**, 123907 (2006).
[7]R. Welter, I. Ijaali, G. Venturini, and P. Malaman, J. Alloys Compd. **265**, 196 (1998).
[8]O. I. Bodak, E. I. Gladyshevskii, and P. I. Kripyakevich, J. Struct. Chem. **11**, 283 (1970).
[9]H. R. Krishna-Murthy and C. Jayaprakash, Phys. Rev. B **30**, 2806 (1984).
[10]See, e.g., A. J. Millis, Phys. Rev. B **48**, 7183 (1993).
[11]H.-U. Desgranges and K. D. Schotte, Phys. Lett. **91A**, 240 (1982).
[12]M. E. Fisher, Philos. Mag. **7**, 1731 (1962).
[13]B. Chevalier, S. F. Matar, M. Ménétrier, J. Sanchez Marcos, and J. Rodriguez Fernandez, J. Phys.: Condens. Matter **18**, 6045 (2006).